This is not the final peer-reviewed Version of Record; 10.1042/etls20170167

Dating the Late Proterozoic Stratigraphic Record

Galen P. Halverson[1,2]
Susannah M. Porter[3]
Timothy M. Gibson[1]

1. Department of Earth and Planetary Sciences, McGill University, 3450 University St., Montréal QC, H3A 0E8 Canada
2. Earth Dynamics Research Group, ARC Centre of Excellence for Core to Crust Fluid Systems (CCFS) and The Institute for Geoscience Research (TIGeR), School of Earth and Planetary Sciences, Curtin University, GPO Box U1987, WA 6845, Australia
3. Department of Earth Science, University of California at Santa Barbara, Santa Barbara, CA 93106, USA

Abstract

The Tonian and Cryogenian periods (1000–635.5 Ma) witnessed important biological and paleoclimatic events, including diversification of eukaryotes, the rise of alga as primary producers, the possible origin of Metazoa, and a pair of Snowball Earth glaciations. The Tonian and Cryogenian periods will also be the next in the geological time scale to be formally defined. Age-calibrating this interval is essential for properly ordering and interpreting these events and establishing and testing hypotheses for paleoenvironmental change. Here we briefly review the methods by which the Proterozoic time scale is dated and provide an up-to-date compilation of age constraints on key fossil first and last appearances, events, and horizons during the Tonian and Cryogenian periods. We also develop a new age model for a ca. 819–740 Ma composite section in Svalbard, which is unusually complete and contains a rich Tonian fossil archive. This model provides useful preliminary age estimates for the Tonian succession in Svalbard and distinct carbon isotope anomalies that can be globally correlated and used as an indirect dating tool.

Dating the geological record is essential for piecing together and interpreting the events and processes that shaped Earth over its 4.54 billion-year history. One way in which geologists tell time is through establishing the order in which events took place through application of the laws of superposition and cross-cutting relationships. These basic yet powerful tools for telling *relative time*, combined with biostratigraphy, enabled early geologists to formulate the framework of a geological time scale long before methods for determining precise ages had been developed[1,2]. However, accurate and precise ages are required to establish rates of processes and calibrate unique events in Earth's history to absolute time[3,4].

Radiometric techniques have been applied to dating geological materials since the pioneering work of Arthur Holmes over a century ago[5]. These techniques exploit a series of different isotopic systems in which a radioactive parent isotope decays into a stable daughter isotope. Many different radiometric dating methods are now regularly employed on a variety of materials[6], and their utility and precision are steadily improving with better constraints on decay constants[7], modification of sample preparation procedures to diminish extrinsic sources of error (e.g., *ref. 8–10*), and development of increasingly sophisticated and highly spatially resolved *in situ* analytical approaches[11]. These radiometric methods, combined with biostratigraphy, magnetostratigraphy, astrochronology, and other tools for correlating rocks globally, have calibrated a highly functional *chronostratigraphic* geological time scale (GTS) for most of the Phanerozoic Eon (541 million years ago [Ma] to present)[12].

Despite the great progress in calibrating and refining the GTS, telling time in the Proterozoic Eon (2500–541 Ma) remains a formidable challenge[4,13]. The difficulty lies partly in the limited utility of biostratigraphy and magnetostratigraphy in rocks of this age, compounded by a fragmentary and typically deformed sedimentary record. Fortunately, a rapidly growing database of geologically well-constrained radiometric ages (Figure 1; SI), combined with chemostratigraphy, provides for an ever-improving geochronological framework for the Proterozoic Eon. Consequently, certain events in Proterozoic Earth history, such as the onset of the Great Oxidation Event (ca. 2420 Ma[14]) and the end of the second (Marinoan) Snowball glaciation (ca. 635.5 Ma[15–17]) are reasonably well dated. Other important events, such as the first appearance of animals and the massive ca. 570 Ma Shuram negative carbon isotope anomaly in the middle

Ediacaran Period, remain poorly dated[18–21]. The aim of this contribution is to provide a brief review of the methods by which the Proterozoic sedimentary record is temporally calibrated, along with updated age constraints on key biological and geological events in the middle to late Proterozoic (ca. 1050 to 635 Ma), which spans the proliferation of complex eukaryotes and a second Proterozoic oxygenation event[22]. A well-resolved time scale is essential to reconcile the processes responsible for the interconnected changes in the biosphere, oceans, atmosphere, paleogeography, and climate during this key interval in Earth's history.

The mineral zircon dated by the uranium-lead (U-Pb) method is the gold standard of radiometric dating techniques. This zirconium silicate mineral ($ZrSiO_4$) crystallizes at high temperatures in felsic magmas and is an ideal geochronometer for multiple reasons. First, it incorporates uranium in trace amounts (100s to 1000s of ppm), but does not incorporate lead, the ultimate daughter product of uranium decay, thus minimizing the need to correct for initial lead in the mineral in age calculations. Second, zircon is a highly durable mineral that can withstand the abuses of volcanic eruptions and multiple weathering and erosion cycles while retaining an isotopic imprint of its origin. Finally, because two separate isotopes of uranium (^{235}U and ^{238}U) decay to two different isotopes of lead (^{207}Pb and ^{206}Pb, respectively), ages can be calculated from three distinct isotopic ratios ($^{207}Pb/^{206}Pb$, $^{207}Pb/^{235}U$, $^{206}Pb/^{238}U$), providing a powerful internal check on the reliability of the ages. Pre-screening (e.g., via imaging by secondary electron microscopy and cathodoluminescence) to select the highest quality zircons, chemical pre-treatment to remove mineral domains that are damaged and prone to lead loss[8], and standardization of isotopic tracers and inter-laboratory calibrations, have led to great improvements in the precision and accuracy of U-Pb ages[23].

The U-Pb isotopic data used to calculate ages are typically acquired via one of three analytical approaches: isotope dilution thermal ionization mass spectrometry (ID-TIMS), secondary ion mass spectrometry (SIMS, which includes the sensitive high-resolution ion microprobe, or SHRIMP), or laser ablation inductively coupled plasma mass spectrometry (LA-ICP-MS). The latter two methods involve *in situ* analyses, which are rapid and can target different domains within individual zircons that may have grown at different times—and hence have different ages. These advantages make *in situ* methods powerful and highly applicable to a wide range of geological problems. However, the precision of the ID-TIMS method, which entails dissolution and analysis of a population of individual zircons (now commonly pre-screened by LA-ICP-MS), yields analytical uncertainties that are 1–2 orders of magnitude better—now as low as ~0.01% or as low as ±100,000 years for zircons of late Proterozoic age[23]. The high precision attainable by the ID-TIMS method makes it the benchmark for calibrating the GTS and individual events in Earth's history[3].

An important caveat in applying the U-Pb zircon method to date the sedimentary record is that it requires finding appropriate rock types: typically felsic to intermediate volcanic lava flows and air fall tuffs (i.e., resulting from explosive eruptions) intercalated with sedimentary strata. These volcanic rocks are not ubiquitous, for they are linked to specific tectonic settings, mainly continental arcs and rift basins. Many passive margin and intracratonic basins, which dominate the middle to late Proterozoic sedimentary record[24], lack volcanic interbeds suitable for U-Pb zircon dating. And even where ostensibly appropriate volcanogenic beds do occur, there is no assurance that they will contain primary, dateable zircons.

Detrital zircon geochronology entails dating a large number of zircons (typically through *in situ* analyses) that have been eroded from other sources and concentrated in sandstones and provides an alternative approach to refining the possible age of poorly dated sedimentary sequences by establishing the maximum possible age of a rock[25]. In some cases, these maximum ages, combined with minimum ages established by other dating techniques, provide valuable age constraints. Even when these data do not contribute meaningfully to dating stratigraphic sequences, they can be a powerful tool for studying sediment provenance and global tectonic cycles (e.g., *26, 27*) and their possible links to global environmental change[28 29].

Another radiometric technique that has gained traction for dating the late Proterozoic record is the rhenium-osmium (Re-Os) isotope system (^{187}Re-^{187}Os) applied to organic-rich rocks. Rhenium and osmium are platinum group elements that occur in low abundance in the continental crust but are relatively enriched in oxygenated seawater. Rhenium and osmium are also organophilic and so hydrogenous phases of both elements occupy chelating sites on organic complexes and are concentrated in organic-rich sediments during deposition and early diagenesis, typically in anoxic settings[30–33]. Selective leaching approaches that liberate only the hydrogenous Re-Os fraction in sediments[34,35], along with normalized isotopic spikes, and analytical techniques that allow measurement of increasingly minute quantities of Re and Os[10,36,37], have greatly improved the reliability of this technique. Importantly, closed system behavior of sedimentary rhenium and osmium has been shown to endure hydrocarbon maturation, demonstrating that the Re-Os geochronometer is impervious to temperature and pressure conditions up to greenschist facies[38].

Although the precision in Re-Os ages (~1%) is much lower than that achievable with U-Pb, a series of recent studies have shown that the technique yields consistent ages[10,36,37]. A striking result of the application of Re-Os geochronology to the Proterozoic fossil record was a major revision to the age of the fossil red alga *Bangiomorpha pubescens* in Arctic Canada, the oldest taxonomically resolvable eukaryote[39] and hence a key calibration point in molecular clock analyses of early eukaryotic evolution[40–42]. Whereas earlier estimates based variably on geological considerations and less robust radiometric dating methods implied an age close to 1200 Ma for *B. pubescens*, a pair of Re-Os ages bracketing its occurrence in the Bylot Supergroup, Baffin Island, constrain its age to 1045 ±15 Ma, with important implications for the timing of primary plastid endosymbiosis[43].

A flurry of recent U-Pb and Re-Os ages from key stratigraphic sections globally that span the ca. 720–635 Ma Cryogenian period (which will soon be formally defined as the oldest period in the GTS behind the ca. 635–540 Ma Ediacaran Period[44]) have demonstrated remarkable consistency in the age of two Cryogenian (Sturtian and Marinoan) snowball glaciations globally (Fig. 1; Supplementary Information). For example, the onset of the Sturtian glaciation is now tightly constrained to have begun between 717.5 and 716.5 Ma based on U-Pb zircon ID-TIMS ages acquired on volcanic rocks just below and just above the basal glacial contact in the Ogilvie Mountains, Yukon[50,51]. Similarly, U-Pb zircon ages from the Marinoan glacial deposits[15] and overlying *cap carbonates* deposited in the immediate aftermath of Snowball glaciation[16] date the boundary between the Cryogenian and Ediacaran periods to 636.6 to 634.2 Ma. This boundary— a so-called *xenoconformity* marking an abrupt global shift in environment[52]— is placed at the base of the cap carbonate and widely considered to be globally synchronous. Because it is an easily identifiable contact and occurs widely (it is known from every continent but Antarctica[53]), this boundary is a unique calibration point in the geological record[54].

Importantly, the radiometric ages bracketing the beginning and end of the Cryogenian glaciations (see Table S1) provide a positive test for one of the key predictions of the Snowball Earth hypothesis—long duration (millions of years) and synchronous onset and end to glaciation[49,55].These ages also serve to calibrate the Cryogenian non-glacial interlude (i.e., ca. 660–640 Ma) between the Sturtian and Marinoan *cryochrons* (Fig. 1), a critical interval in Earth's history, which includes the first biomarker evidence for sponges[56] and putative fossil evidence for predatory Rhizaria[57] (Table 1). In increase in the abundance of the C_{27}, C_{28}, and C_{30} steranes and sterane/hopane ratios during this interlude also indicate the rise to dominance of eukaryotic algae as primary producers[68].

Due to the vagaries of the geological record, certain sedimentary successions and time intervals are especially well dated, such as the latest Tonian to early Cryogenian of northwestern Canada, the southwestern USA, and South China (Table S1). Others are not. The Tonian period (1000 to ca. 720 Ma as currently defined[44]) overall is poorly calibrated radiometrically. Furthermore, the Tonian sedimentary succession in Svalbard, perhaps the best preserved and most complete in the world for this time period[69,70] and a critical archive of important fossil[39,60,62,71–73] and geochemical[69,74–78] data has not been directly dated. In the absence of direct radiometric ages, easily identified GTS boundaries or biostratigraphic zonation (e.g., *ref. 63,76*), other approaches are required to tell time in this and other successions for this time interval.

Chemostratigraphic correlation is one such tool with great utility in the Neoproterozoic Era[79]. Chemostratigraphy relies on sedimentary materials, such as carbonate minerals or organic carbon, that can be treated as dependable proxies for the isotopic composition of the seawater in which they form. Using chemostratigraphy for correlation requires the additional assumptions that the isotope system of interest is globally uniform in seawater (i.e., that it is has a long residence time relative to the mixing time of the ocean) and can be reliably preserved in the rock record. Commonly applied chemostratigraphic proxies for the Proterozoic Eon include carbon ($\delta^{13}C$), sulfur ($\delta^{34}S$), and strontium ($^{87}Sr/^{86}Sr$) isotope ratios. Carbon isotope ratios are particularly useful in the Neoproterozoic because of the high amplitude and low frequency fluctuations that characterize this time period (Fig. 1) and the abundance of well-preserved carbonate successions. Although the Neoproterozoic Era was a time of generally high average $\delta^{13}C$ values (+5‰), a series of deep negative $\delta^{13}C$ anomalies punctuates this record (Fig. 1). Some of these anomalies are temporally and causally closely associated with Neoproterozoic glaciations[69,79], whereas others are not. For example, the so-called Bitter Springs Anomaly (BSA; Figs. 1, 2), named after the eponymous formation in the Amadeus basin of central Australia, is well defined in early–middle Neoproterozoic basins globally[65,69,81,82], where it can be confidently linked to the same global seawater perturbation based on broad age constraints, other chemostratigraphic data (namely $^{87}Sr/^{86}Sr$[75]), and its uniquely symmetric beginning and end (Fig. 2). In the Fifteenmile Group of northwestern Canada, a U-Pb zircon date on a volcanic tuff[50] and a Re-Os date on organic-rich rocks[46] provide maximum age constraints on the onset of the BSA of 811.51±0.25 Ma and 815.29±5.2 Ma, respectively. U-Pb ages zircon dates of 815.29±0.32 Ma and 778.72±0.24 Ma on tuffs above and below the BSA in the Tambien Group of Ethiopia[65] are consistent with those from NW Canada and provide additional control on the duration of the anomaly. These ages can be used to tell time indirectly in other, undated successions, such as the Akademikerbreen Group in Svalbard, through chemostratigraphic correlation (Fig. 2).

A second Tonian negative carbon isotope anomaly occurs in the upper Russøya Member of Svalbard, above the Akademikerbreen Group and just below the Cryogenian (Sturtian) Petrovbreen Member glacial deposits (Fig. 2). Whereas this negative carbon isotope anomaly had previously been linked to the onset of Cryogenian glaciation[80], new Re-Os age determinations bracketing the likely correlative negative $\delta^{13}C$ anomaly in northwestern Canada (the Coppercap anomaly[36,66]) imply that it precedes the onset of Cryogenian glaciation by >15 m.y. (Fig. 1). Through a combination of sequence stratigraphic and chemostratigraphic correlation, these ages can be applied to the late Tonian strata in Svalbard[70] (Fig. 2). In an analogous way, data from other successions of overlapping age and completeness, can be mapped onto this composite stratigraphic column and used to calibrate Tonian time.

These and other correlated ages can further be used to develop a height-age model for the Tonian stratigraphic succession in Svalbard. Where viable, subsidence models, which invoke the tectonic mechanism for the generation of sedimentary basins, provide more geologically realistic and accurate age-height relationships than simple linear interpolation between known (or assumed) ages. When plotted against composite stratigraphic height, the Svalbard ages fall on an exponentially decreasing curve (Fig. 3). This height-age relationship is predicted for thermally subsiding basins whose subsidence is the result of cooling of lithosphere previously stretched by extension[83]. Sediment-loaded thermal subsidence curves can be calculated as a function of a stretching factor (β) based on the solution to the heat flow equation, using physical parameters for the lithosphere, such as its thickness, density, and thermal conductivity. An assumption is also required for where in the stratigraphic column thermal subsidence begins. Although the tectonic context for the origin of the Neoproterozoic basin in Svalbard is not well understood[70], the contact between siliciclastic sediments of the Veteranen Group below and platformal carbonates of the Akademikerbreen Group above is a reasonable approximation for the rift–drift transition in Svalbard[84] and is borne out by a systematic relationship between age and stratigraphic height (Fig. 3). The best-fit subsidence curve for these data yields β = 1.263 and t_0 = 819.3 Ma for the onset of rifting (i.e., the Veteranen–Akademikerbreen contact).

This subsidence age model estimates the timing of key stratigraphic horizons within the Svalbard stratigraphic succession such as the onset (810 Ma) and end (802 Ma) of the Bitter Springs Anomaly and the boundary between the Akademikerbreen and Polarisbreen groups (752 Ma). It also provides age estimates for the local first appearance datum (FAD) and last appearance datum (LAD) and of the possible index fossils *Trachyshystrichosphaera aimika* (805–795 Ma) and *Cerebrosphaera globosa* (802–782 Ma), respectively (Table 1). The oldest putative chlorophytes *Proterocladus* and *Palaeastrum dyptocranum*[60], the possible stramenopile *Jacutianema solubila*[72], and the oldest amoebozoans[59,62,54,86] all also occur in the Tonian strata of Svalbard and can be assigned model ages (Table 1; Fig. 2). Dates for other important Tonian–Cryogenian body fossil and molecular fossil first occurrences—such as apatite scale microfossils[46], possible Rhizaria[57] and ciliates[64], and the 24-isopropylcholestane sponge biomarker[56]—are also estimated based on available radiometric ages on the successions in which the fossils were found or easily correlated equivalents (Table 1).

These age assignments should not be treated as validation of the taxonomic interpretation of these fossils. Rather, they should be combined with complementary approaches to querying and quantifying the biostratigraphic record. Constrained optimization (CONOP) was recently applied to estimating Tonian–Cryogenian species richness[73], highlighting that the record is now sufficiently resolved to apply biochronological and other statistical approaches. Indeed, radiometric dating techniques alone are insufficient for precise calibration of the GTS[87]. Whereas linear interpolation and spline-fitting techniques have traditionally been used for estimating ages of GTS boundaries in the Phanerozoic record[12], this approach is being superseded by Bayesian statistical modelling, which is well suited to incorporating the many uncertainties intrinsic to dating the stratigraphic record[87,88]. The Proterozoic record presents unique challenges to applying these approaches, but an important first step is to construct composite stratigraphic sections onto which available chronostratigraphic data can be mapped[89], such as the Tonian–Cryogenian section of Svalbard (Fig. 2). In this way, the Proterozoic GTS will gradually be filled in and provide the chronological framework within which we may interpret the extraordinary events that ushered in habitable Phanerozoic world.

Figure 1. (A) The Geological Time Scale (GTS) spanning the Neoproterozoic Era (modified from *ref. 12*), along with a compilation of the carbonate Neoproterozoic $\delta^{13}C$ record (modified from *ref. 45*), with negative carbon isotope anomalies particularly useful for chemostratigraphic correlations noted (BSA = Bitter Springs Anomaly; CA = Coppercap anomaly; TA = Trezona Anomaly; SA = Shuram Anomaly). Fossil cartoons indicate (from bottom to top), first appearance of algae[39,43], apatite scale microfossils[46], the large ornamented Ediacaran microfossils[47], and the Ediacaran biota[48]. Note that only the Ediacaran Period is formally defined chronostratigraphically, but the Cryogenian period will soon be formalized and the chronometrically defined Tonian period will likely be revised and subdivided chronostratigraphically[44]. GSSP refers to formally defined global stratotype section and point period boundaries. (B) The Sturtian and Marinoan (M) cryochrons (Snowball Earth events) during the Cryogenian period with positions (open boxes) of the radiometric dates that constraint their durations and appear to confirm their synchronous onsets and terminations (see also *ref.*

49). Black squares are zircon and baddeleyite ID-TIMS dates, grey squares are in situ (SHRIMP and SIMS) dates, and purple squares are Re-Os dates. See Table 1 for age estimates for the onset and end of the cryochrons based on these dates and SI Table 1 for a compilation of all of the dates, including their errors and literature sources.

Figure 2. A composite stratigraphic column through the Akademikerbreen Group and lower Polarisbreen Group (Russøya Member) of the Hecla Hoek Series of northeastern Svalbard (modified from *ref. 70*). Grey circles represent all available carbonate carbon isotope data for the succession mapped onto the composite stratigraphic column (from *refs. 69,70,80* and previously unpublished data), and the solid line a LOESS smoothing fit to these data. Approximate stratigraphic position of radiometric ages (in Ma) that can be confidently correlated into the Akademikerbreen–Russøya section are shown in arrows (see SI Table 1 for sources of data), along with subsidence model ages (in Ma) for important stratigraphic heights, including the base of the Akademikerbreen Group, the onset and end of the Bitter Springs δ^{13}C anomaly, and the Akademikerbreen-Polarisbreen contact. Stratigraphic LAD and FAD are for key fossil occurrences in Svalbard. See Table 1 for references and additional ages. Note that the LAD of the VSM is only loosely constrained to be within the Russøya Mb.

Figure 3. One dimensional McKenzie-type[83] sediment-loaded thermal subsidence models for the long-term evolution of the East Svalbard basin (e.g., *ref. 69*) using the stratigraphic record of the Akademikerbreen Group and Russøya Member and correlated ages (open squares with age and approximate stratigraphic uncertainties). The key assumptions in the model are that thermal subsidence began with the base of the Akademikerbreen Group, which corresponds to the onset of nearly continuous carbonate deposition[84], there was no major erosional unconformity in the succession, and that carbonate cementation occurred shortly after sedimentation (additional details on the application of this type of model to carbonate platforms can be found in *ref. 85*). The unconstrained parameters are the stretching factor (β) and the timing of onset of thermal subsidence (open diamond; t_0); these were optimized using a chi-squared test. The resulting best fit (t_0 = 819.3; β = 1.263; $p > 0.999$) was then used to generate an age model for the entire Akademikerbreen Group and Russøya Member. Additional subsidence curves for β = 1.25 and 1.30 shown for comparison.

Table 1. Summary of key events, horizons, and biostratigraphic ranges, and first and last appearance data for the latest Mesoproterozoic to Cryogenian geological record that can be reliably estimated based on available radiometric ages and/or the subsidence-age model (Fig. 3) for the latter Tonian stratigraphic succession in Svalbard. See Table S2 for additional ages for stratigraphic heights and formation and member boundaries in Svalbard.

References

1. Williams, H.S., 1893. The making of the Geological Time-Scale. *J. Geol.* **1**, 180–197.
2. Morrell, J. (2001) Genesis and geochronology: the case of John Phillips (1800–1874). In C.L.E. and S. J. Knell (Eds.) The Age of the Earth: from 4004 BC to AD 2002. Geo. Soc. London, Sp. Pubs., **190**, 85–90.
3. Schmitz, M.D. (2012) Radiogenic isotope geochronology. In Gradstein, F.M., Ogg, J.O., Schmitz, M.D., and Ogg, G. (Eds.) *The Geological Time Scale 2012*, Elsevier, 114–126.
4. Knoll, A. H., and Nowak, M. A. (2017). The timetable of evolution. *Science advances* **3**, e1603076.
5. Holmes, A. (1911) Association of lead with uranium in rock minerals and its application to the measurement of geological time. *P. R. Soc. London* **85**, 248–256.
6. Rink, W.J., and Thompson, J.W. (2015). Encyclopedia of Scientific Dating Methods. Encyclopedia of Earth Sciences Series, Springer Reference (Dordrecht).
7. Condon, D. J., Schoene, B., McLean, N.M., Bowring, S.A., and Parrish, R.R. (2015). Metrology and traceability of the U-Pb isotope dilution geochronology (EARTHTIME Tracer Calibration Part I). *Geochim. Cosmochim. Acta* **164**, 464–480.
8. Mattinson, J.M. (2005) Zircon U-Pb chemical abrasion (“CA-TIMS”) method: Combined annealing and multi-step partial dissolution analysis for improved precision and accuracy of zircon ages. *Chem. Geol*. **200**, 47–66.
9. Schmitz, M.D. and Schoene, B. (2007) Derivation of isotope ratios, errors, and error correlations for U-Pb geochronology using ^{205}Pb-^{235}U-(^{233}U)-spiked isotope dilution thermal ionization mass spectrometric data. Geochem. *Geophys. Geosys.* **8**, 10.1029/2006GC001492.
10. Rooney, A.D., Austermann, J., Smith, R.F., Li, Y., Selby, D., Dehler, C.M., Schmitz, M.D., Karlstrom, K. E., and Macdonald, F. A. (2018). Coupled Re-Os and U-Pb geochronology of the Tonian Chuar Group, Grand Canyon. *Geol. Soc. Am. Bull.* 10.1130/B31768.1.
11. Nemchin, A.A., Horstwood, M.S.A., and Whitehouse, M.J. (2013) High-spatial resolution geochronology. *Elements* **9**, 31–39.
12. Gradstein, F.M., Ogg, J.G., Schmitz, M.D., and Ogg, G.M. (2012) *The Geological Time Scale 2012*. Elsevier (Amsterdam).
13. Knoll, A. H. (2000) Learning to tell Neoproterozoic time. *Precambrian Res*. **100**, 3–20.
14. Gumsley, A.P., Chamberlain, K.R., Bleeker, W., Söderland, U., de Kock, M.O., Larsson, E.R., and Bekker, A. (2017) Timing and tempo of the Great Oxidation Event. *P. Natl. Acad. Sci. USA* **114**, 1811–1816.

15. Hoffmann, K.H., Condon, D.J., Bowring, S.A., and Crowley, J.L. (2004) A U-Pb zircon date from the Neoproterozoic Ghaub Formation, Namibia: Constraints on Marinoan glaciation. *Geology* **32**, 817–820.
16. Condon, D., Zhu, M., Bowring, S., Jin, Y., Wang, W., and Yang, A. (2005). From the Marinoan glaciation to the oldest bilaterians: U-Pb ages from the Doushantuo Formation, China. *Science* **308**, 95–98.
17. Calver, C.R., Crowley, J.L., Wingate, M.T.D., Evans, D.A.D., Raub, T.D., and Schmitz, M.D. (2013) Globally synchronous Marinoan deglaciation indicated by U-Pb geochronology of the Cottons Breccia, Tasmania, Australia. *Geology*, **41**, 1127–1130.
18. Pell, S. D., McKirdy, D. M., Jansyn, J., and Jenkins, R. J. F. (1993) Ediacaran carbon isotope stratigraphy of South Australia — an initial study. *Trans. Royal Soc. S. Austr.* **117**, 153–161.
19. Burns, S., Haudenschild, U., and Matter, A. (1994) The strontium isotopic composition of carbonates from the Late Precambrian (~560–540 Ma) Huqf Group of Oman. *Chem. Geol*. **111**, 269–282.
20. Grotzinger, J.P., Fike, D.A., and Fischer, W.W. (2011) Enigmatic origin of the largest-known carbon isotope excursion in Earth's history. *Nat. Geosc*. **4**, 285–292.
21. Husson, J.M., Maloof, A.C., and Schoene, B. (2012) A syn-depositional age for Earth's deepest $\delta^{13}C$ excursion required by isotope conglomerate tests. *Terra Nova* **24**, 318–325.
22. Lyons, T.W., Reinhard, C.T., and Planavsky, N.J. (2014). The rise of oxygen in Earth's early ocean and atmosphere. *Nature* **506**, 307–315.
23. Schmitz, M.D. and Kuiper, K.F. (2013) High-precision geochronology. *Elements* **9**, 25–30.
24. Bradley, D. C. (2011) Secular trends in the geologic record and the supercontinent cycle. *Earth-Science Reviews*, **108**, 16-33.
25. Dickinson, W. R., and Gehrels, G. E. (2009). Use of U–Pb ages of detrital zircons to infer maximum depositional ages of strata: a test against a Colorado Plateau Mesozoic database. *Earth Planet. Sc. Lett.* **288**, 115-125.
26. Voice, P.J., Kowalewski, M., Eriksson, K.A. (2011) Quantifying the timing and rate of crustal evolution: Global compilation of radiometrically dated detrital zircon grains. *J. Geol.* **119**, 109–126.
27. Cawood, P.A., Hawkesworth, C.J., and Dhuime, B. (2013) The continental record and the generation of continental crust. *Geol. Soc. Am. Bull.* **125**, 14–32.
28. McKenzie, N.R., Horton, B.K., Loomis, S.E., Stockli, D.F., Planavsky, N.J., and Lee, C.-T. (2016) Continental arc volcanism as the principal driver of icehouse-greenhouse variability. *P. Nat. Ac. Sci. (USA)* **352**, 444–447.
29. Lee, C.-T., Yeung, L.Y., McKenzie, N.R., Yukoyama, Y., Ozaki, K., 2016. Two-step rise of atmospheric oxygen linked to the growth of continents. *Nat. Geosc.* **9**, 417–424.
30. Ravizza, G. and Turekian, K.K. (1988). Application of the ^{187}Re-^{187}Os system to black shale geochronometry. *Geochim. Cosmochim. Acta* **53**, 3257–3262.
31. Colodner, D., Sachs, J., Ravizza, G., Turekian, K., Edmond, J. and Boyle, E. (1993) The geochemical cycle of rhenium: a reconnaissance. *Earth Plan. Sc. Lett*. **117**, 205–221.
32. Crusius, J., Calvert, S., Pedersen, T., and Sage, D. (1996) Rhenium and molybdenum enrichments in sediments as indicators of oxic, suboxic, and sulfidic conditions of deposition. *Earth Planet. Sc. Lett*. **145**, 65–78.
33. Yamashita, Y., Takahashi, Y., Haba, H., Enomoto, S. and Shimizu H. (2007). Comparison of reductive accumulation of Re and Os in seawater–sediment systems. *Geochim. Cosmochim. Acta* **71**, 3458–3475.

34. Selby, D., and Creaser, R.A. (2003) Re-Os geochronology of organic rich sediments: an evaluation of organic matter analysis methods. *Chem. Geo*. **200**, 225–240.
35. Kendall, B., Creaser, R. A., Calver, C. R., Raub, T. D., and Evans, D. A. D. (2009) Correlation of Sturtian diamictite successions in southern Australia and northwestern Tasmania by Re-Os black shale geochronology and the ambiguity of "Sturtian"-type diamictite-cap carbonate pairs as chronostratigraphic marker horizons. *Precambrian Res.* **172**, 301–310.
36. Rooney, A.D., Macdonald, F.A., Strauss, J.V., Dudás, F.Ö., Hallmann, C., and Selby, D. (2014). Re-Os geochronology and coupled Os-Sr isotope constraints on the Sturtian snowball Earth. *P. Nat. Ac. Sci. (USA)* **111**, 51–56.
37. Rooney, A.D., Strauss, J.V., Brandon, A.D., and Macdonald, F.A. (2015) A Cryogenian chronology: Two long-lasting synchronous Neoproterozoic glaciations. *Geology* **43**, 459–462.
38. Creaser, R.A., Sannigraha, P., Chacko, T., and Selby, D. (2002) Further evaluation of the Re-Os geochronometer in organic-rich sedimentary rocks: A test of hydrocarbon maturation effects in the Exshaw Formation, Western Canada Sedimentary Basin. *Geochim. Cosmochim. Acta* **66**, 3441–3452.
39. Butterfield, N.J. (2000) *Bangiomorpha pubescens* n. Gen., n. sp.: Implications for the evolution of sex, multicellularity, and the Mesoproterozoic/Neoproterozoic radiation of eukaryotes. *Paleobiology* **26** 386–404, https://doi.org/10.1666/0094.
40. Berney, C., and Pawlowski, J. (2006) A molecular time-scale for eukaryote evolution recalibrated with the continuous microfossil record. *Royal Society of London Philosophical Transactions, Ser. B*, **273**, 1867–1872.
41. Parfrey, L.W., Lahr, D.J.G., Knoll, A.H., and Katz, L.A. (2011) Estimating the timing of early eukaryotic diversification with multigene molecular clocks. *P. Nat. Ac. Sci. (USA)* **108**, 13,624–13,629.
42. Eme, L., Sharpe, S.C., Brown, M.W., and Roger, A.J. (2014) On the age of eukaryotes: Evaluating evidence from fossils to molecular clocks. *Cold Spring Harbor Persp. Bio.* **6**, a016139, https://doi.org/10.1101/cshperspect.a016139.
43. Gibson, T.M., Shih, P.M., Cumming, V.M., Fischer, W.W., Crockford, P.W., Hodgskiss, M.S.W., Wörndle, S., Creaser, R.A., Rainbird, R.H., Skulski, T.M., and Halverson, G.P. (2018) Precise age of *Bangiomorpha pubescens* dates the origin of eukaryotic photosynthesis. *Geology* **46**, 135–139.
44. Shields-Zhou, G., Porter, S. A., and Halverson, G. P. (2016) A new rock-based definition for the Cryogenian Period (circa 720 – 635 Ma). Episodes **39**, 3–9.
45. Cox, G. M., Halverson, G. P., Stevenson, R. K., Vokaty, M., Poirier, A., Kunzmann, M., Li, Z.-X., Denyszyn, S. W., Strauss, J. V., and Macdonald, F. A. (2016) Continental flood basalt weathering as a trigger for Neoproterozoic Snowball Earth. *Earth Plan. Sci. Lett.* **446**, 89–99.
46. Cohen, P.A., Strauss, J.V., Rooney, A.D., Sharma, M., and Tosca, N. (2017) Controlled hydroxyapatite biomineralization in an ~810 million-year-old unicellular eukaryote. *Science Advances* **3**, e1700095.
47. Cohen, P.A., Knoll, A.H., and Kodner, R.B. (2009) Large spinose microfossils in Ediacaran rocks as resting stages of early animals. *P. Natl. Acad. Sci. USA* **106**, 6519–6524.
48. Narbonne, G.M. (2004) Modular construction of early Ediacaran complex life forms. *Science* **305**, 1141–1144.

49. Hoffman, P.F., Abbott, D.S., Ashkenay, Y., Benn, D. I., Brocks, J.J., Cohen, P.A., Cox, G.M., Creveling, J.R., Donnadieu, Y., Erwin, D.H., Fairchild, I.J., Ferreira, D., Goodman, J.C., Halverson, G.P., Jansen, M.F., Le Hir, G., Love, G.D., Macdonald, F.A., Maloof, A.C., Partin, C.A., Ramstein, G., Rose, B.E.J., Rose, C.V., Sadler, P.M., Tziperman, E., Voigt, A., and Warren, S.G. (2017) Snowball Earth climate dynamics and Cryogenian geology and geobiology. *Science Advances* **3**, e1600983.
50. Macdonald, F.A., Schmitz, M.D., Crowley, J.L., Roots, C.F., Jones, D.S., Maloof, A.C., Strauss, J.V., Cohen, P.A., Johnston, D.T., and Schrag, D.P. (2010) Calibrating the Cryogenian. *Science* **327**, 1241–1243.
51. Macdonald, F.A., Schmitz, M.D., Strauss, J.V., Halverson, G.P., Gibson, T.M., Eyster, A., Cox, G., Mamrol, P., and Crowley, J.L. (2017). Cryogenian of Yukon. *Precambrian Res.*, in press, 10.1016/j.precamres.2017.08.015.
52. Carroll, A.R. (2017) Xenoconformities and the stratigraphic record of paleoenvironmental change. *Geology* **45**, 639–642.
53. Hoffman, P. F. and Li, Z. X. (2009) A palaeogeographic context for Neoproterozoic glaciation. *Palaeogeog. Palaeoclim. Palaeoec.* **277**, 158–172.
54. Halverson, G.P. (2017) Introducing the Xenoconformity. *Geology* **45**, 671–672.
55. Hoffman, P.F., Kaufman, A.J., Halverson, G.P., and Schrag, D.P. (1998) A Neoproterozoic snowball Earth. *Science* **281**, 1342–1346.
56. Love, G.D., Grosjean, E., Stalvies, C., Fike, D. A., Grotzinger, J.P., Bradley, A.S., Kelly, A.E., Bhatia, M., Meredith, W., Snape, C. E., Bowring, S.A., Condon, D.J., and Summons, R.E. (2009) Fossil steroids record the appearance of Demosponges during the Cryogenian period. *Nature* **457**, 718–721.
57. Bosak, T., Lahr, D.J.G., Pruss, S.B., Macdonald, F.A., Gooday, A.J., Dalton, L., and Matys, E. D. (2012) Possible early foraminiferas in post-Sturtian (716–635 Ma) cap carbonates. *Geology*, **40**, 67–70.
58. Knoll, A.H., Wörndle, S., and Kah, L.C. (2013) Covariance of microfossil assemblages and microbialite textures across an upper Mesoproterozoic carbonate platform. *Palaios* **28**, 453–470.
59. Knoll, A.H., Swett, K., and Mark, J. (1991) Paleobiology of a Neoproterozoic tidal flat/lagoonal complex: The Draken Conglomerate Formation, Spitsbergen. *J. Paleont*. **65**, 531–570.
60. Butterfield, N. J., Knoll, A. H., and Swett, K. (1994). Paleobiology of the Neoproterozoic Svanbergfjellet Formation, Spitsbergen. *Fossils and Strata* **34**, 1–81.
61. Martí Mus, M. (2001) Palaeobiology and taphonomy of early problematic fossil (Ph.D. dissertation). Uppsala University.
62. Riedman, L.A., Porter, S.M., and Calver, C.R. (2017). Vase-shaped microfossil biostratigraphy with new data from Tasmania, Svalbard, Greenland, Sweden and the Yukon. Precambrian Research, page 10.1016/j.precamres.2017.09.019.
63. Cox, G.M., Isakson, V., Hoffman, P.F., Gernon, T.M., Schmitz, M.F., Shain, S., Collins, A.S., Preiss, W., Blades, M.L., Mitchell, R.N., and Nordsvan, A. (in review) U-Pb zircon (CA-ID-TIMS) age supports globally synchronous Sturtian deglaciation. *Precambrian Res.*
64. Bosak, T., Lahr, D.J.G., Pruss, S.B., Macdonald, F.A., Dalton, L., and Matys, E. (2011) Aggutinated tests in post-Sturtian cap carbonates of Namibia and Mongolia. *Earth Planet. Sc. Lett.*, **308**, 29–40.

65. Swanson-Hysell, N. L., Maloof, A. C., Condon, D. J., Jenkin, G. R. T., Alene, M., Tremblay, M. M., Tesema, T., Rooney, A. D., and Haileab, B (2015) Stratigraphy and geochronology of the Tambien Group, Ethiopia: Evidence for globally synchronous carbon isotope change in the Neoproterozoic. *Geology* **43**, 323–326.
66. Strauss, J.V., Rooney, A.D., Macdonald, F.A., Brandon, A.D., and Knoll, A.H. (2014) 740 Ma base-shaped microfossils from Yukon, Canada: Implications for Neoproterozoic chronology and biostratigraphy 740 Ma vase-shaped microfossils from Yukon, Canada: Implications for Neoproterozoic chronology and biostratigraphy. *Geology* **42**, 659–662.
67. Prave, A.R., Condon, D.J., Hoffmann, K.H., Tapster, S., and Fallick, A.E. (2016) Duration and nature of the end-Cryogenian (Marinoan) glaciation. *Geology* **44**, 631–634.
68. Brocks, J.J., Jarrett, A.J.M., Sirantoine, E., Hallmann, C., Hoshino, Y., and Liyanage, T. (2017) The rise of algae in Cryogenian oceans and the emergence of animals. *Nature* **548**, 578–581.
69. Halverson, G.P., Hoffman, P.F., Schrag, D.P., Maloof, A.C., and Rice, A.H. (2005) Towards a Neoproterozoic composite carbon isotope record. *Geol. Soc. Am. Bull.* **117**, 1181–1207.
70. Halverson, G.P., Kunzmann, M., Strauss, J.V., Maloof, A.C. (2017) The Tonian-Cryogenian transition in Svalbard. *Precambrian Res.* DOI: 10.1016/j.precamres.2017.12.010.
71. Knoll, A.H. (1982) Microfossil-based biostratigraphy of the Precambrian Hecla Hoek sequence, Nordaustlandet, Svalbard. *Geol. Mag.* **119**, 269–279.
72. Butterfield, N. J. (2004). A vaucheriacean alga from the middle Neoproterozoic of Spitsbergen: implications for the evolution of Proterozoic eukaryotes and the Cambrian explosion. *Paleobiology* **30**, 231–251.
73. Riedman, L.A. and Sadler, P.M. (2017) Global species richness record and biostratigraphic potential of early to middle Neoproterozoic eukaryote fossils. *Precambrian Research*. (doi:doi.org/10.1016/j.precamres.2017.10.008).
74. Knoll, A.H., Hayes, J.M., Kaufman, A.J., Swett, K., and Lambert, I.B. (1986) Secular variation in carbon isotope ratios from Upper Proterozoic successions of Svalbard and east Greenland. *Nature* **321**, 832–837.
75. Halverson, G.P., Dudás, F.Ö., Maloof, A.C., and Bowring, S.A. (2007) Evolution of the $^{87}Sr/^{86}Sr$ composition of Neoproterozoic seawater. *Palaeogeog. Palaeoclim. Palaeoec*. 256, 103–129.
76. Kunzmann, M., Bui, T.H. Crockford, P.W, Halverson, G.P., Scott, C., Lyons, T.W., and Wing, B.A. (2017) Bacterial sulfur disproportionation constrains timing of Neoproterozoic oxygenation. *Geology* **45**, 207–210.
77. Kunzmann, M., Gibson, T.M., Halverson, G.P., Hodgskiss, M.S.W., Bui, T.H., Carozza, D.A., Sperling, E.A., Poirier, A., Cox, G.M., and Wing, B.A. (2017) Iron isotope biogeochemistry of Neoproterozoic marine shales. *Geochim. Cosmochim. Acta*, 209, 85–105.
78. Kunzmann, M., Halverson, G.P., Scott, C., Minarik, W.G., and Wing, B.A. (2015) Geochemistry of Neoproterozoic black shales from Svalbard: Implications for oceanic redox conditions spanning Cryogenian glaciations. *Chem. Geol.* **417**, 383--393.
79. Kaufman, A. J., Knoll, A. H., and Narbonne, G. M. (1997) Isotopes, ice ages, and terminal Proterozoic Earth history. *P. Nat. Acad. Sci. USA* **95**, 6600–6605.
80. Hoffman, P.F., Halverson, G.P., Domack, E.W., Maloof, A.C., Swanson-Hysell, N.L., and Cox, G.M. (2012) Cryogenian glaciations on the southern tropical paleomargin of Laurentia (NE Svalbard and East Greenland), and a primary origin for the upper Russøya (Islay) carbon isotope excursion. *Precambrian Res*. **206-207**, 137–158.

81. Hill, A. C. and Walter (2000) Mid-Neoproterozoic (~830–750 Ma) isotope stratigraphy of Australia and global correlation. *Precambrian Res.* **100**, 181–211.
82. Thomson, D., Rainbird, R. H., Planavsky, N., and Lyons, T. W. (2015) Chemostratigraphy of the Shaler Supergroup, Victoria Island, NW Canada: A record of ocean composition prior to the Cryogenian glaciations. *Precambrian Res.* **263**, 232–245.
83. McKenzie, D. (1978) Some remarks on the development of sedimentary basins. *Earth Planet. Sci. Lett.,* 40, 25–32.
84. Maloof, A.C., Halverson, G.P., Kirschvink, J.L., Schrag, D.P., Weiss, B., and Hoffman, P.F. (2006). Combined paleomagnetic, isotopic and stratigraphic evidence for true polar wander from the Neoproterozoic Akademikerbreen Group, Svalbard. *Geol. Soc. Am. Bull.* **118**, 1099–1124.
85. Halverson, G.P, Hoffman, P.F., Kaufman, A.J., and Schrag, D.P. (2002) A major perturbation of the carbon cycle before the Ghaub glaciation (Neoproterozoic) in Namibia: prelude to snowball Earth? *Geochem. Geophys. Geosys.* **3**, 10.1029/2001GC000244.
86. Porter, S.M. and Knoll, A.H. (2000) Testate amoebae in the Neoproterozoic Era: evidence from vase-shaped microfossils in the Chuar Group, Grand Canyon. *Paleobiology* **26**, 360-385.
87. De Vleeschouwer, D. and Parnell, A.C. (2014) Reducing time-scale uncertainty for the Devonian by integrating astrochonology and Bayesian statistics. *Geology* **42**, 491–494.
88. Parnell, A.C., Buck, C.E., and Doan, T.K. (2011) A review of statistical chronology models for high-resolution Holocene palaeoenvironmental reconstruction. *Quatern. Sci. Rev.* **30**, 2948–2960.
89. Saddler, P.M. (2006) Composite time lines: a means to leverage resolving power from radioisotopic dates and biostratigraphy. *Paleont. Soc. Papers* **12**, 145–170.

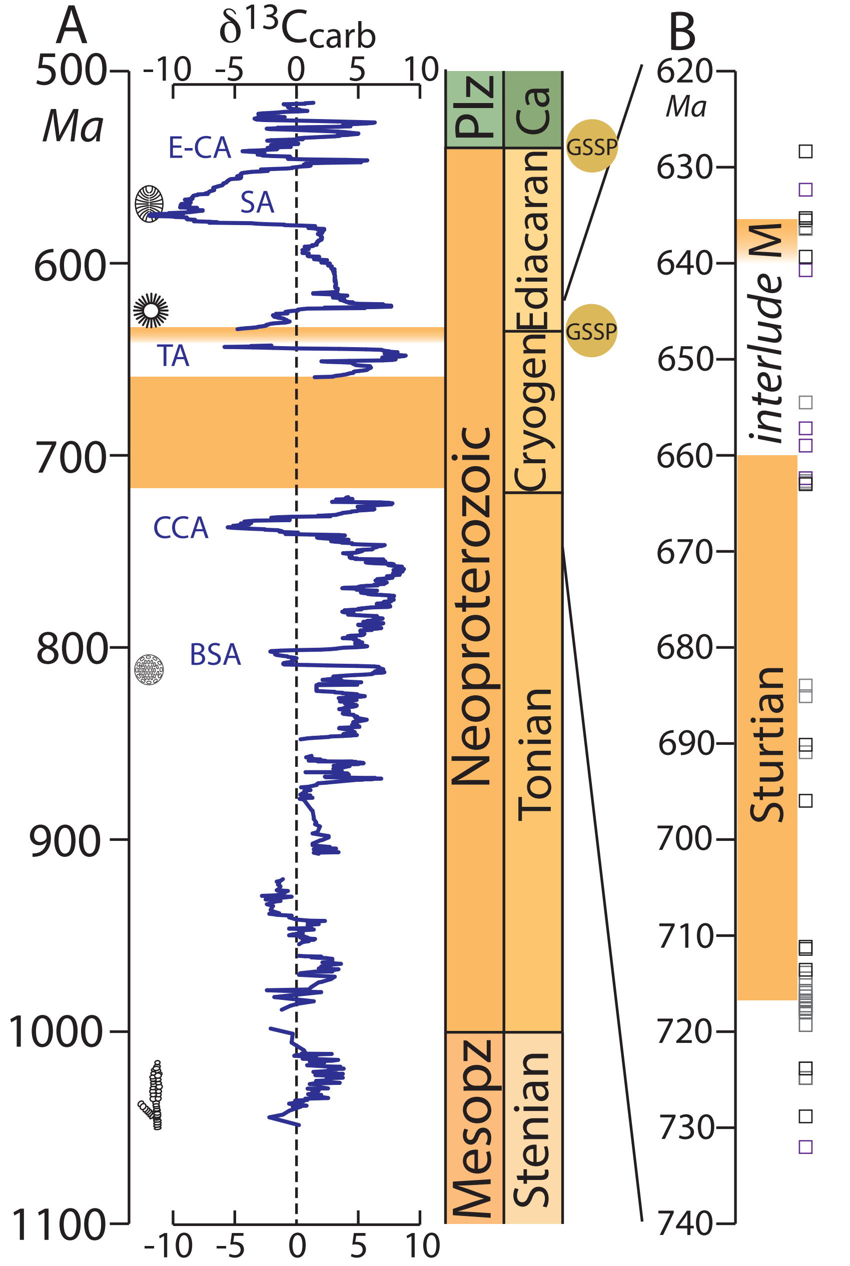
A
δ13Ccarb
500
Ma
600
700
800
900
1000
1100
-10
-5
0
5
10
E-CA
SA
TA
CCA
BSA
Plz
Ca
Ediacaran
Cryogen
Neoproterozoic
Tonian
Mesopz
Stenian
GSSP
GSSP
B
620
Ma
630
640
650
660
670
680
690
700
710
720
730
740
interlude M
Sturtian

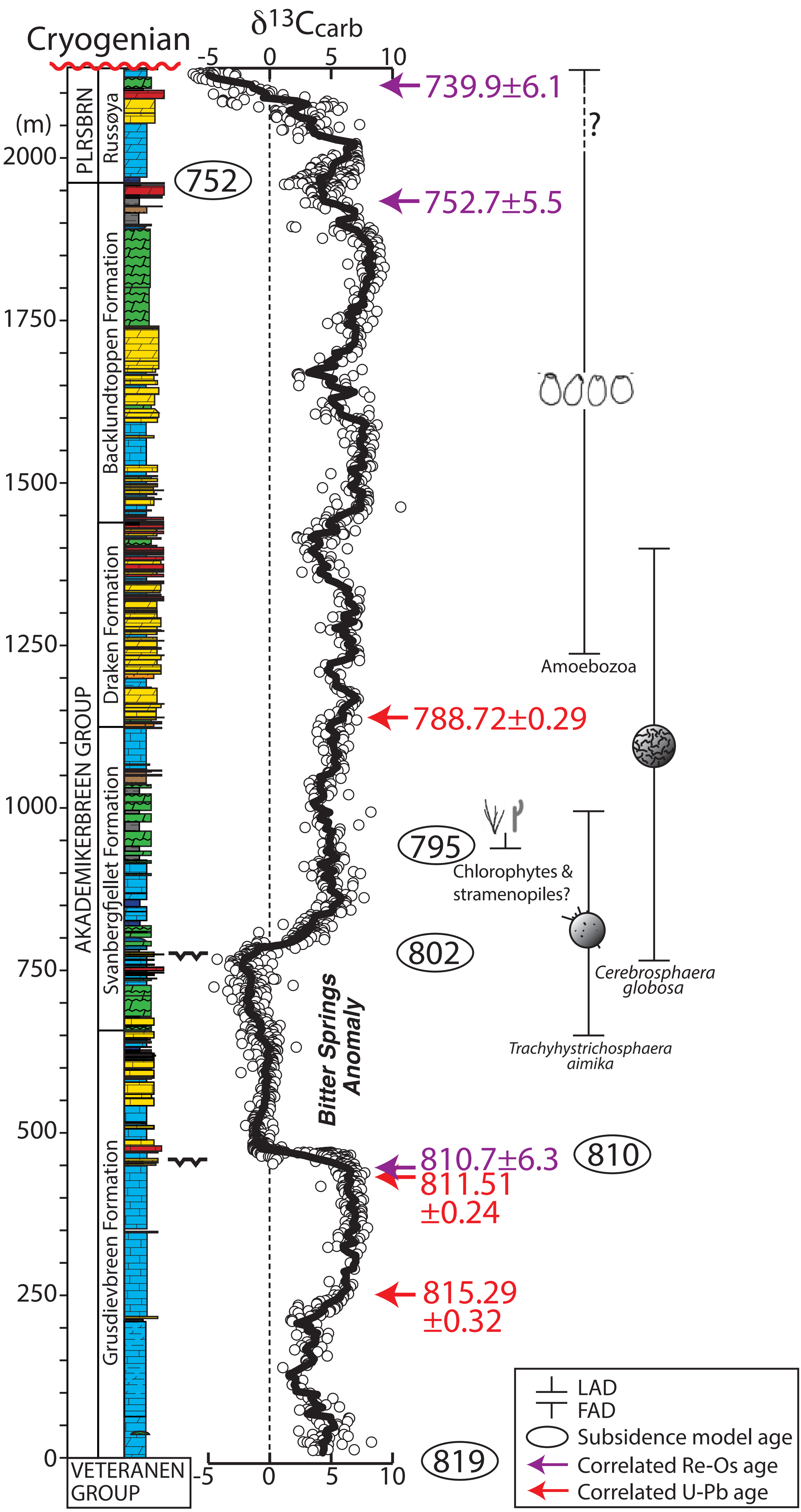

Cryogenian
δ13Ccarb
-5 0 5 10
(m)
2000
1750
1500
1250
1000
750
500
250
0
PLRSBRN
Russøya
AKADEMIKERBREEN GROUP
Backlundtoppen Formation
Draken Formation
Svanbergfjellet Formation
Grusdievbreen Formation
VETERANEN GROUP
752
795
802
810
819
739.9±6.1
752.7±5.5
788.72±0.29
810.7±6.3
811.51 ±0.24
815.29 ±0.32
?
Amoebozoa
Chlorophytes & stramenopiles?
Cerebrosphaera globosa
Trachyhystrichosphaera aimika
Bitter Springs Anomaly
LAD
FAD
Subsidence model age
Correlated Re-Os age
Correlated U-Pb age

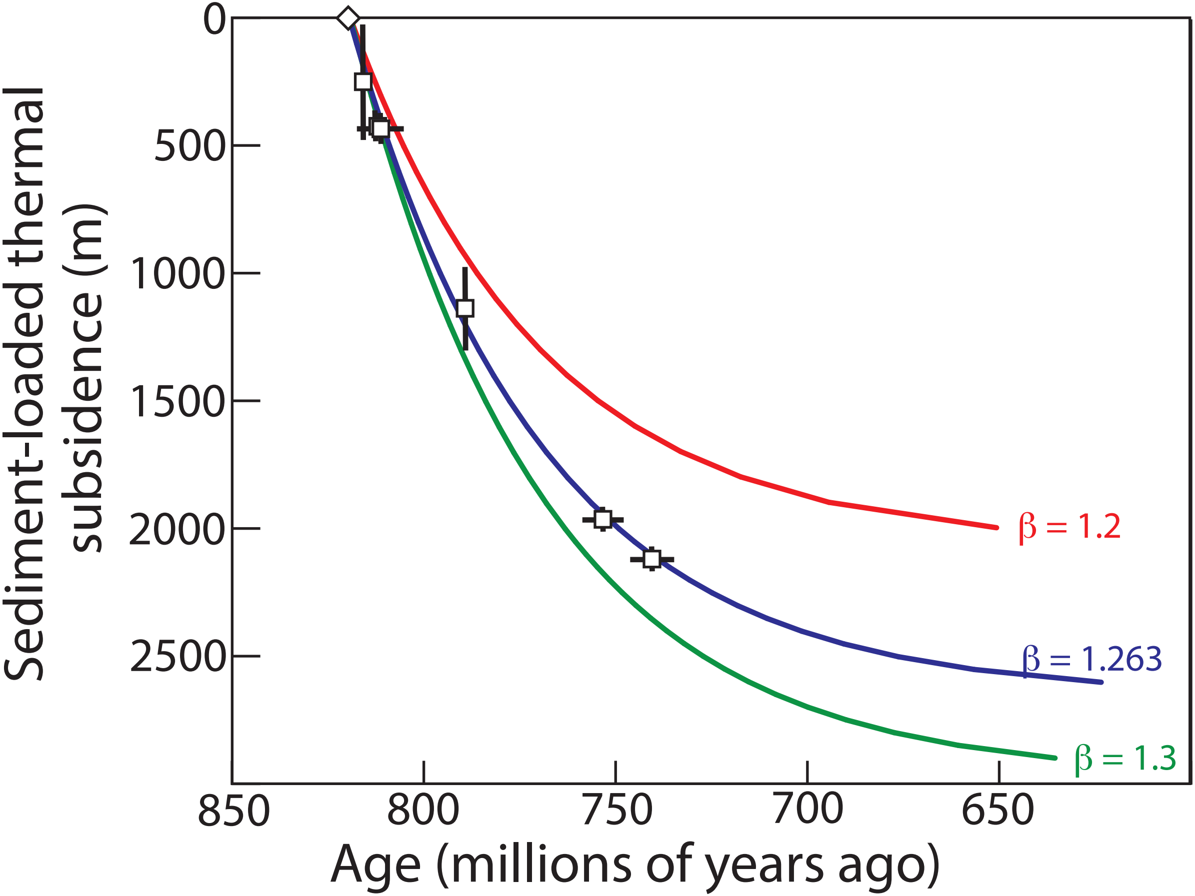

Sediment-loaded thermal subsidence (m)
0
500
1000
1500
2000
2500
850
800
750
700
650
Age (millions of years ago)
β = 1.2
β = 1.263
β = 1.3

Event, FAD, LAD, or stratigraphic range	**Date**	**Method**	**References**
Rhodophyta (*Bangiomorpha pubescens*) (FAD)	1045 ± 15 Ma	Re-Os	39, 43, 58
Apatite scale microfossils (FAD)	810.7 ±5.8 Ma	Re-Os	46
*Trachyhystrichosphaera aimika**	ca. 805–795 Ma	Subsidence model age	59, 60
*Cerebrosphaera globosa**	ca. 802–782 Ma	Subsidence model age	60
?Chlorophyta (*Palaeastrum, Proterocladus)** (FAD)	ca. 795 Ma	Subsidence model age	60
Amoebozoa*	ca. 787 Ma	Subsidence model age	61, 62
?Rhizaria (FAD)	ca. 660 Ma	U-Pb CA-TIMS + correlation	57, 63
?Tintinnids (FAD)	ca. 660 Ma	U-Pb CA-TIMS + correlation	63, 64
Sponge biomarkers	660–639 Ma	U-Pb CA-TIMS + correlation	56, 63
Base of Akademikerbreen Group	ca. 819 Ma	Subsidence model age	
Onset of Bitter Springs Anomaly	ca. 810 Ma	U-Pb, Re-Os, subsidence model age	46, 50, 65
End of Bitter Springs Anomaly	ca. 802 Ma	Subsidence model age	
Coppercap δ^{13}C anomaly minimum	ca. 738 Ma	Re-Os, subsidence model age	66
Onset Sturtian glaciation	ca. 717 Ma	U-Pb	50, 51
End Sturtian glaciation	ca. 660 ma	U-Pb, Re-Os	63
Onset Marinoan glaciation	ca. 640 Ma	U-Pb	67
End Maronian glaciation/base Ediacaran Period	ca. 635.5 Ma	U-Pb	15–17

*In Svalbard

Table S1.
Summary of age constraints on the begin and end of the Cryogenian glaciations and the Bitter Springs anomaly.

Table S2.
Ages for stratigraphic heights and formation/member boundaries generated using the thermal subsidence model for the Akademikerbreen–Russøya succession.

References

Baldwin, G. J., Turner, E. C., and Kamber, B. Z. (2016) Tectonic controls on distribution and stratigraphy of the Cryogenian Rapitan iron formation, northwestern Canada. *Precambrian Res.* **278**, 303–322.

Bowring, S. A., Grotzinger, J. P., Condon, D. J., Ramezani, J., Newall, M. J., and Allen, P. A. (2007) Geochronological constraints on the chronostratigraphic framework of the Neoproterozoic Huqf Superroup, Sultanate of Oman. *Am. J. Sci.* **307**, 1097–1145.

Calver, C.R., Crowley, J.L., Wingate, M.T.D., Evans, D.A.D., Raub, T.D., and Schmitz, M.D. (2013) Globally synchronous Marinoan deglaciation indicated by U-Pb geochronology of the Cottons Breccia, Tasmania, Australia. *Geology*, **41**, 1127–1130.

Cohen, P.A., Strauss, J.V., Rooney, A.D., Sharma, M., and Tosca, N. (2017). Con- trolled hydroxyapatite biomineralization in an ∼810 million-year-old unicellular eukaryote. *Science Advances* **3**, e1700095.

Condon, D., Zhu, M., Bowring, S., Jin, Y., Wang, W., and Yang, A. (2005). From the Marinoan glaciation to the oldest bilaterians: U-Pb ages from the Doushantuo Formation, China. *Science* **308**, 95–98.

Cox, G.M., Isakson, V., Hoffman, P.F., Gernon, T.M., Schmitz, M.F., Shain, S., Collins, A.S., Preiss, W., Blades, M.L., Mitchell, R.N., and Nordsvan, A. (in review) U-Pb zircon (CA-ID-TIMS) age supports globally synchronous Sturtian deglaciation. *Precambrian Res.*

Cox, G.M., Strauss, J.V., Halverson, G.P., Schmitz, M.D., McClelland, W.C., Stevenson, R.S., and Macdonald, F.A. (2015) Kikiktat volcanics of Arctic Alaska—Melting of harzburgitic mantle associated with the Franklin large igneous province. *Lithosphere* **7**, 275–295.

Eyster, A., Ferri, F., Schmitz, M. D., and Macdonald, F. A. (2018) One diamictite and two rifts: Stratigraphy and geochronology of the Gataga Mountain of northern British Columbia. *Am. J. Sci.* **318**, 167–207.

Fanning, C. and Link, P. (2004) U-Pb SHRIMP ages of Neoproterozoic (Sturtian) glaciogenic Pocatello Formation, southeastern Idaho. *Geology* **32**, 881–884.

Hoffmann, K.H., Condon, D.J., Bowring, S.A., and Crowley, J.L. (2004) A U-Pb zircon date from the Neoproterozoic Ghaub Formation, Namibia: Constraints on Marinoan glaciation. *Geology* **32**, 817–820.

Kendall, B., Creaser, R. A., and Selby, D. (2006) Re-Os geochronology of postglacial black shales in Australia: Consequences for timing of the Sturtian glaciation. *Geology* **34**, 729–732.

Kendall, B., Creaser, R. A., Calver, C. R., Raub, T. D., and Evans, D. A. D. (2009) Correlation of Sturtian diamictite successions in southern Australia and northwestern Tasmania by Re-Os black shale geochronology and the ambiguity of "Sturtian"-type diamictite-cap carbonate pairs as chronostratigraphic marker horizons. *Precambrian Res.* **172**, 301–310.

Lan, Z., Li, X., Zhu, M., Chean, Z.-Q., Zhang, Q., Li, Q., Lu, D., Liu, Y., and Tang, G. (2014) A rapid and synchronous initiation of the wide spread Cryogenian glaciations. *Precambrian Res.* **255**, 401–411.

Lan, Z., Li, X.-H., Zhang, Q., and Li, Q.-L. (2015a) Global synchronous initiation of the 2nd episode of Sturtian glaciation: SIMS zircon U–Pb and O isotope evidence from the Jiangkou Group, South China. *Precambrian Res.* **267**, 28–38.

Lan, Z., Li, X.-H., Zhu, M., Zhang, Q., and Li, Q.-L. (2015b). Revisiting the Liantuo Formation in Yangtze Block, South China: SIMS U–Pb zircon age constraints and regional and global significance. *Precambrian Res.* **267**, 123–141.

Lund, K., Aleinikoff, J.N., Evans, K.V., and Fanning, C. (2003) SHRIMP U-Pb geochronology of Neoproterozoic Windermere Supergroup, central Idaho: Implications for rifting of western Laurentia and synchroneity of Sturtian glacial deposits. *Geol. Soc. Am. Bull.* **115**, 349–372.

Lund, K., Aleinikoff, J.N., Evans, K.V., duBray, E.A., Dewitt, E.H., and Unrah, D.M. (2010) SHRIMP U-Pb dating of recurrent Cryogenian and Late Cambrian–Early Ordovician alkalic magmatism in central Idaho: Implications for Rodinian rift tectonics. *Geol. Soc. Am. Bull.* **122**, 430–453.

Macdonald, F.A., Schmitz, M.D., Crowley, J.L., Roots, C.F., Jones, D.S., Maloof, A.C., Strauss, J.V., Cohen, P.A., Johnston, D.T., and Schrag, D.P. (2010) Calibrating the Cryogenian. *Science* **327**, 1241–1243.

Macdonald, F.A., Schmitz, M.D., Strauss, J.V., Halverson, G.P., Gibson, T.M., Eyster, A., Cox, G., Mamrol, P., and Crowley, J.L. (2017) Cryogenian of Yukon. *Precambrian Res.*, in press, 10.1016/j.precamres.2017.08.015.

Prave, A.R., Condon, D.J., Hoffmann, K.H., Tapster, S., and Fallick, A.E. (2016) Duration and nature of the end-Cryogenian (Marinoan) glaciation. *Geology* **44**, 631–634.

Rooney, A.D., Austermann, J., Smith, R.F., Li, Y., Selby, D., Dehler, C.M., Schmitz, M.D., Karlstrom, K. E., and Macdonald, F. A. (2018). Coupled Re-Os and U-Pb geochronology of the Tonian Chuar Group, Grand Canyon. *Geol. Soc. Am. Bull.* 10.1130/B31768.1.

Rooney, A.D., Macdonald, F.A., Strauss, J.V., Dudás, F.Ö., Hallmann, C., and Selby, D. (2014). Re-Os geochronology and coupled Os-Sr isotope constraints on the Sturtian snowball Earth. *P. Nat. Ac. Sci. (USA)* **111**, 51–56.

Rooney, A.D., Strauss, J.V., Brandon, A.D., and Macdonald, F.A. (2015) A Cryogenian chronology: Two long-lasting synchronous Neoproterozoic glaciations. *Geology* **43**, 459–462.

Schmitz, M.D. (2012) Radiogenic isotope geochronology. In Gradstein, F.M., Ogg, J.O., Schmitz, M.D., and Ogg, G. (Eds.) *The Geological Time Scale 2012*, Elsevier, 114–126.

Song, G., Wang, X., Shi, X., and Jiang, G. (2017) New U-Pb age constraints on the upper Banxi Group and synchrony of the Sturtian glaciation in South China. *Geosc. Frontiers* **8**, 1161–1173.

Swanson-Hysell, N. L., Maloof, A. C., Condon, D. J., Jenkin, G. R. T., Alene, M., Tremblay, M. M., Tesema, T., Rooney, A. D., and Haileab, B (2015) Stratigraphy and geochronol- ogy of the Tambien Group, Ethiopia: Evidence for globally synchronous carbon isotope change in the Neoproterozoic. *Geology* **43**, 323–326.

Tollo, R. P. and Aleinikoff, J. N. (1996) Petrology and U-PB geochronology of the Robertson River Igneous Suite, Blue Ridge province, Virginia - Evidence for multistage magmatism associated witn an early episode of Laurentian rifting. American Journal of Science, 296:1045–1090.

Xu, B., Xiao, S., Zou, H., Chen, Y., Li, Z.-X., Song, B., Liu, D., Zhou, C., and Yuan, X. (2009) SHRIMP zircon U-Pb age constraints on Neoproterozoic Quruqtagh diamictites in NW China. *Precambrian Res*. **168**, 247–258.

Yu, W., Algeo, T. J., Du, Y., Zhou, Q., Wang, P., Xu, Y., Yuan, L., and Pan, W. (2017). Newly discovered Sturtian cap carbonate in the Nanhua Basin, South China. Precambrian Research, 293:112–130.

Zhang, Q.-R., Li, X.-H., Feng., L.-J., Huang, J., and Song, B. (2008a) A new age constraint on the onset of Neoproterozoic glaciations in the Yangze Platform, South China. *The Journal of Geology* **116**, 423–429.

Zhang, S., Jiang, G., and Han, Y. (2008b) The age of the Nantuo Formation and Nantuo glaciation in South China. *Terra Nova* **20**, 289–294.

Zhang, S., Jiang, G., Zhang, J., Song, B., Kennedy, M., and Christie-Blick, N (2005). U-Pb sensitive high-resolution ion microprobe ages from the Doushantuo Formation in south China: Constraints on late Neoproterozoic glaciations. *Geology* **33**, 473–476.

Zhou, C., Tucker, R., Xiao, S., Peng, Z., Yuan, X., and Chen, Z. (2004) New constraints on the ages of Neoproterozoic glaciations in south China. *Geology* **32**, 437–440.

Event	Age	Error	Technique	Max/Min	Location	Reference
Onset/End Bitter Springs Anomaly*	815.29	±0.32	U-Pb zircon CA-ID-TIMS	max	Ethiopia	Swanson-Hysell et al. (2015)
	811.51	±0.25	U-Pb zircon CA-ID-TIMS	max	Yukon, Canada	Macdonald et al. (2010)
	810.7	±6.3	Re-Os	max	Yukon, Canada	Cohen et al. (2018)
	778.72	±0.24	U-Pb zircon CA-ID-TIMS	min	Ethiopia	Swanson-Hysell et al. (2015)
	777.38	±0.14	U-Pb zircon CA-ID-TIMS	min	Ethiopia	Swanson-Hysell et al. (2015)
Onset Sturtian glaciation	732.2	±3.9	Re-Os	max	NWT, Canada	Rooney et al. (2014)
	729	±0.9	U-Pb zircon CA-ID-TIMS	max	SW USA	Rooney et al. (2018)
	725.0	±10	U-Pb zircon SHRIMP	max	South China	Xu et al. (2009)
	725.0	±10	U-Pb zircon SHRIMP	max	South China	Zhang et al. (2008)
	724.0	±3.0	U-Pb zircon ID-TIMS	max	Viriginia, USA	Tollo and Aleinikoff (1996)
	719.47	±0.29	U-Pb zircon CA-ID-TIMS	max	Alaska, USA	Cox et al. (2015)
	718.1	±0.3	U-Pb zircon CA-ID-TIMS	max	Yukon, Canada	Macdonald et al. (2018)
	718.1	±0.2	U-Pb zircon CA-ID-TIMS	max	Yukon, Canada	Macdonald et al. (2018)
	717.8	±0.2	U-Pb zircon CA-ID-TIMS	max	Yukon, Canada	Macdonald et al. (2018)
	717.7	±0.3	U-Pb zircon CA-ID-TIMS	max	Yukon, Canada	Macdonald et al. (2018)
	717.43	±0.14	U-Pb zircon CA-ID-TIMS	max	Yukon, Canada	Macdonald et al. (2010)
	717.0	±4.0	U-Pb zircon SHRIMP	max	Idaho, USA	Fanning & Link (2004)
	716.9	±0.4	U-Pb zircon CA-ID-TIMS	min	Yukon, Canada	Macdonald et al. (2018)
	716.47	±0.24	U-Pb zircon CA-ID-TIMS	min	Yukon, Canada	Macdonald et al. (2010)
	716.1	±3.4	U-Pb zircon SIMS	max	South China	Lan et al. (2014)
	715.9	±2.8	U-Pb zircon SIMS	max	South China	Lan et al. (2014)
	714.6	±5.2	U-Pb zircon LA-ICPMS	max	South China	Song et al. (2017)
	714.0	±8.0	U-Pb zircon SHRIMP	max	South China	Lan et al. (2015)
	711.52	±0.2	U-Pb zircon CA-ID-TIMS	min	Oman	Bowring et al. (2007)
	711.3	±0.3	U-Pb zircon CA-ID-TIMS	min	NWT, Canada	Baldwin et al. (2016)
End Sturtian glaciation	696.2	±0.2	U-Pb zircon CA-ID-TIMS	max	Northern BC	Eyster et al. (2018)
	691	±12	U-Pb zircon SIMS	max	South China	Lan et al. (2015b)
	690.1	±0.2	U-Pb zircon CA-ID-TIMS	max	Northern BC	Eyster et al. (2018)
	685	±7	U-Pb zircon SHRIMP	max	Central Idaho	Lund et al. (2003, 2010)
	684	±4	U-Pb zircon SHRIMP	max	Central Idaho	Lund et al. (2003, 2010)
	663.03	±0.11	U-Pb zircon CA-ID-TIMS	max	South Australia	Cox et al. (2018)
	662.9	±4.3	U-Pb zircon SHRIMP	min	South China	Zhou et al. (2004)
	662.7	±6.2	U-Pb zircon LA-ICMPS	min	South China	Yu et al. (2017)
	662.4	±4.3	Re-Os	min	NWT, Canada	Rooney et al. (2014)
	659	±4.5	Re-Os	min	Tuva, Mongolia	Rooney et al. (2015)
	657.2	±6.9	Re-Os	min	Australia	Kendall et al. (2006)
Onset Marinoan glaciation	654.5	±3.8	U-Pb zircon SHRIMP	max	South China	Zhang et al. (2005)
	640.7	±5.7	Re-Os	max	Tasmania, Australia	Kendall et al. (2009)
	639.29	±0.26	U-Pb zircon CA-ID-TIMS	min	Northern Namibia	Prave et al. (2016)
End Marinoan glaciation	636.3	±4.9	U-Pb zircon SHRIMP	max	South China	Zhang et al. (2005)
	635.5	±1.1	U-Pb zircon CA-ID-TIMS	max	Central Namibia	Hoffmann et al. (2004), recalculated by Schmitz et al. (2012)
	636.4	±0.5	U-Pb zircon CA-ID-TIMS	min	Tasmania, Australia	Calver et al. (2013)
	635.26	±1.1	U-Pb zircon CA-ID-TIMS	min	South China	Condon et al. (2004), recalculated by Schmitz et al. (2012)
	632.3	±5.9	Re-Os	min	NWT, Canada	Rooney et al. (2015)

*Age constraints are entirely below onset of Bitter Springs anomaly after end of the anomaly

m	age
2140	736.9
2100	740.6
2050	745.0
2000	749.0
1950	752.7
1900	756.1
1850	759.3
1800	762.4
1750	765.2
1700	767.9
1650	770.5
1600	772.9
1550	775.3
1500	777.5
1450	779.6
1400	781.7
1350	783.6
1300	785.5
1250	787.3
1200	789.1
1150	790.8
1100	792.4
1050	794.0
1000	795.6
950	797.1
900	798.5
850	799.9
800	801.3
750	802.6
700	803.9
650	805.2
600	806.4
550	807.6
500	808.8
450	810.0
400	811.1
350	812.2
300	813.3
250	814.3
200	815.4
150	816.4
100	817.4
50	818.3
0	819.3

Formation	Member	height base (m)	age base (Ma)
lower Elbo-breen Fm.	Petrovbreen Mb.	2130	737.8
	Russøya Mb.	1961	751.9
Backlund-toppen Fm.	Kinnvika Mb.	1894.1	756.5
	Backlundtoppen Fm. (lower)	1439.6	780.0
Draken Fm.		1126	791.6
Svanberg-fjellet Fm.	Upper Limestone member	1059.6	793.7
	Upper Algal Dolomite member	947.1	797.1
	Lower Limestone member	780.2	801.8
	Lower Dolomite member	660	804.9
Grusdiev-breen Fm.	Upper Grusdievbreen member	462	809.7
	Lower Grusdievbreen member	0	819.3